Chalcogenide Letters Vol. 6, No.11, November 2009, p. 583-593

X-RAY POWDER DIFFRACTION STUDY FOR THE $Cu_2Cd_{1-z}Fe_zSnSe_4$ ALLOY SYSTEM

J. A. HENAO, M. A. MACÍAS, M. QUINTERO[a*], E. MORENO[a], M. MOROCOIMA[a], E. QUINTERO[a], P. GRIMA[a], R. TOVAR[a], P. BOCARANDA[a]
Grupo de Investigación en Química Estructural (GIQUE), Facultad de Ciencias, Escuela de Química, Universidad Industrial de Santander, Apartado aéreo 678, Bucaramanga, Colombia.
[a]*Centro de Estudios de Semiconductores, Departamento de Física, Facultad de Ciencias, Universidad de Los Andes, Mérida 5101, Venezuela.*

Room temperature X-ray powder diffraction measurements were carroed out on polycrystalline samples of the $Cu_2Cd_{1-z}Fe_zSnSe_4$ alloy system. The diffraction patterns were used to show the equilibrium conditions and to derive crystalline parameter values. The results confirmed that the alloys are single phase with the tetragonal stannite α ($I\bar{4}2m$) structure. In each case, the crystal structure was refined using the Rietveld method. Values of the atomic parameters were determined as a function of composition z. It was found that the form of the internal distortion σ vs z curve is nonlinear. In addition to the tetragonal stannite α phase extra X-ray diffraction lines due $FeSe_2$ were observe for as grown samples in the range $0.7<z<1.0$. However, it was found that the amount of the extra phase decreased considerably for the compressed samples.

(Received November 6, 2009; accepted November 26, 2009)

Keywords: Magnetic semiconductors, Crystal structure, X-ray powder diffraction, Rietveld refinement.

1. Introduction

Magnetic semiconducting materials (MSM) are of interest because of the manner in which the magnetic behavior associated with the concerned magnetic ion can modify and complement the semiconductor properties [1, 2]. These MSM have received attention because of their potential application in optoelectronic and magnetic devices. Through the use of alloys, the properties of MSM can be tailored by varying the composition to precisely match specific requirements. The materials that have been most studied are the semimagnetic semiconductor alloys obtained from the tetrahedrally coordinated II-VI semiconductor chalcogenide compounds by replacing a fraction of the group II cations with manganese, giving alloys which show spin-glass behavior, very large magneto-optical effects, bound magnetic polarons (BMPs), etc. [1,2]. It was recently suggested [3,4] that another set of magnetic compounds and alloys, which could show larger magneto-optical effect than the II-VI derived chalcogenide alloys, can be obtained from the tetrahedral bonded I_2-II-IV-VI_4 chalcogenide compounds by replacing the II cations with Mn, Fe, Co and/or Ni ions. The crystal structure of various I_2-II-IV-VI_4 chalcogenide compounds has been investigated by several authors [1,3,4,5], and it has been found that in almost all cases, the compounds showed either the tetrahedral tetragonal stannite ($I\bar{4}2m$) structure based on zinc-blende, or an orthorhombic superstructure derived from wurtzite (known as wurtz-stannite, $Pmn2_1$). The general composition diagram for these I_2-II-IV-VI_4 compounds together with its related binary and ternary compounds can be represented by a regular tetrahedron as shown in fig. 1 with I = Cu, II = Cd, Mn and/or Fe, IV = Sn and VI = Se elements at the four apices.

*Corresponding author: mquinter@ula.ve

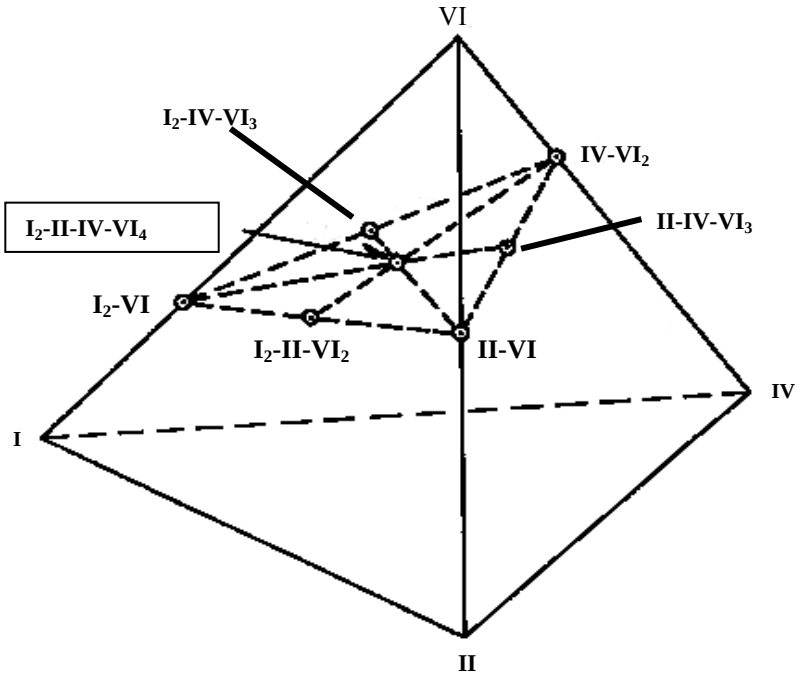

Fig. 1. General composition diagram of the terminal Cu_2-II-Sn-Se_4 compounds with II = Cd and/or Fe. The $Cu_2CdSnSe_4$ and $Cu_2FeSnSe_4$ compounds can be found in the $(Cu_2SnSe_3)_{1-x}(II\text{-}Se)_x$ section at x = 0.5.

With regard to the I_2-II-IV-VI_4 compounds and their alloys, lattice parameter values and phase diagrams for the $Cu_2Cd_{1-z}Mn_zGeSe_4$, $Cu_2Cd_{1-z}Fe_zGeSe_4$ and $Cu_2Zn_{1-z}Fe_zGeSe_4$ chalcogenide alloy systems have been given in earlier works [6, 7]. The magnetic properties of the $Cu_2Cd_{1-z}Mn_zGeSe_4$ and $Cu_2Cd_{1-z}Fe_zGeSe_4$ alloys have been investigated in ref [8]. The X-ray powder diffraction study of the $Cu_2Cd_{1-z}Mn_zSnSe_4$ alloys has been given by Sachanyuk *et al.* [9]. Their results showed that the crystallographic parameter values follow the usual linear Vegard behaviour. In the present work, the $Cu_2Cd_{1-z}Fe_zSnSe_4$ system is being studied, here the results of the crystal structure refinement obtained for this chalcogenide alloy system using the Rietveld method are given.

2. Experimental

The alloy samples were produced by the melt and anneal technique. In each case, the components of 1 g sample were sealed under vacuum ($\approx 10^{-5}$ Torr) in a small quartz ampoule, then heated up to 200 °C and kept for about 1-2 h. Then the temperature was raised to 500 °C using at a rate of 40 K/h, and held at this temperature for 14 hour. After, the samples were heated from 500 °C to 800 °C at 30 K/h and kept at this temperature for another 14 hours, and then the temperature was raised to 1150 °C at 60 K/h, and melted together at this temperature, initially, for about 1 hour. The furnace temperature was brought slowly (4 K/h) down to 600 °C, and the samples were annealed at this temperature for 1 month. Then, the samples were slowly cooled to room temperature using at about 2 K/h. Hence, the resulting as grown samples were investigated by X-ray powder diffraction, with a Rigaku D/MAX IIIB diffractometer equipped with an X-ray tube (CuKα radiation: λ= 1.5406Å; 40 kV, 30 mA) using a diffracted beam graphite monochromator. A

fixed aperture and divergence slit and soller Slit of 1°, a 0.3mm receiving slit and 0.6mm monochromator Reciving Slit were used. The X-ray experimental conditions are summarized in Table 1.

Table 1. Rietveld refinement details for the system $Cu_2Cd_{1-z}Fe_zSnSe_4$.

Molecular formula	$Cu_2Cd_{0.9}Fe_{0.1}SnSe_4$		$Cu_2Cd_{0.8}Fe_{0.2}SnSe_4$		$Cu_2Cd_{0.7}Fe_{0.3}SnSe_4$		$Cu_2Cd_{0.6}Fe_{0.4}SnSe_4$		$Cu_2Cd_{0.5}Fe_{0.5}SnSe_4$
Molecular weight (g/mol)	668.49		662.71		657.18		651.52		645.87
a (Å)	5.8168(1)		5.8050(2)		5.7997(2)		5.7856(2)		5.7726(2)
c (Å)	11.3942(4)		11.3943(4)		11.3802(4)		11.3678(4)		11.3585(5)
V (Å^3)	385.52		383.97		382.79		380.52		378.50
Z	2		2		2		2		2
Space group	$I\bar{4}2m$ (N° 121)		$I\bar{4}2m$ (N° 121)		$I\bar{4}2m$ (N° 121)		$I\bar{4}2m$ (N° 121)		$I\bar{4}2m$ (N° 121)
D_x (g/cm^3)	5.74		5.73		5.66		5.63		5.59
Rw	6.11		6.37		5.90		6.86		5.60
R_B	4.63		4.77		4.51		5.37		4.32
Rexp	3.05		3.05		3.16		3.17		3.19
χ^2	2.00		2.09		1.87		2.16		1.76
Molecular formula	$Cu_2Cd_{0.4}Fe_{0.6}SnSe_4$		$Cu_2Cd_{0.3}Fe_{0.7}SnSe_4$		$Cu_2Cd_{0.2}Fe_{0.8}SnSe_4$		$Cu_2Cd_{0.1}Fe_{0.9}SnSe_4$		$Cu_2FeSnSe_4$
Molecular weight (g/mol)	640.21		634.55		628.78		623.24		617.59
a (Å)	5.7600(3)		5.7480(2)		5.7354 (1)		5.7227(2)		5.7086(2)
c (Å)	11.3408(4)		11.3294(4)		11.3162 (3)		11.2969(4)		11.2786(4)
V (Å^3)	376.26		374.32		372.24		369.97		367.55
Z	2		2		2		2		2
Space group	$I\bar{4}2m$ (N° 121)		$I\bar{4}2m$ (N° 121)		$I\bar{4}2m$ (N° 121)		$I\bar{4}2m$ (N° 121)		$I\bar{4}2m$ (N° 121)
D_x (g/cm^3)	5.56		5.53		5.50		5.45		5.45
Rw	6.62		6.55		7.24		6.67		7.94
R_B	5.13		4.74		5.65		5.24		6.05
Rexp	3.21		3.03		3.20		3.53		3.34
χ^2	2.06		2.16		2.26		1.89		2.38

λ	CuK_α (1.5406 Å)		Step size 2θ (°)	0.02
Temperature (K)	295(1)		Counting time (s)	6
Data range 2θ (°)	2-70		N°. step intensities	3400
Nº refined parameters	21		Peak-shape profile	Pseudo-Voigt

The X-ray diffraction patterns, obtained for each sample, were indexed with the computer program DICVOL04 [10] using an absolute error of 0.03° (2θ) in the calculations. The space group was established using CHECKCELL program [11]. The resulting parameter values were refined using the NBS'AIDS program [12]. It is to be mentioned that, in the range $0.7<z<1.0$, for as grown samples, few extra lines were observed in the diffraction pattern and these were found to be due to the presence of small amounts $FeSe_2$ as a secondary phases. Each sample, showing to be two

phase, was carefully crushed and the final powder was compressed in a new quartz ampoule. Then, the compressed sample was re-melted at 1150 ºC for about 3-4 h, and the annealing procedure indicated above was repeated. It was found that, for most of the compressed samples, the intensities of the extra diffraction lines were considerably reduced, and no sensible variation of lattice parameter values of the main phase was observed for the as grown and compressed samples, both giving similar parameter values. However, the observation of small traces of any extra phase was complemented with magnetic susceptibility measurements using a Quantum Design MPMS-5 SQUID magnetometer. These magnetic measurements showed that the amount of $FeSe_2$ for the compressed samples were considerably smaller than for the as grown samples. A typical example of this is illustrated in fig. 2, where the variations of the inverse of the magnetic susceptibility $1/\chi$ with temperature T, for as grown and compressed samples with z=1 ($Cu_2FeSnSe_4$), are shown. It is seen from this figure that the $1/\chi$ vs T curve obtained for the as grown sample shows a broad minimum around 250 K due to the presence of the secondary $FeSe_2$ phase observed in the X-ray results.

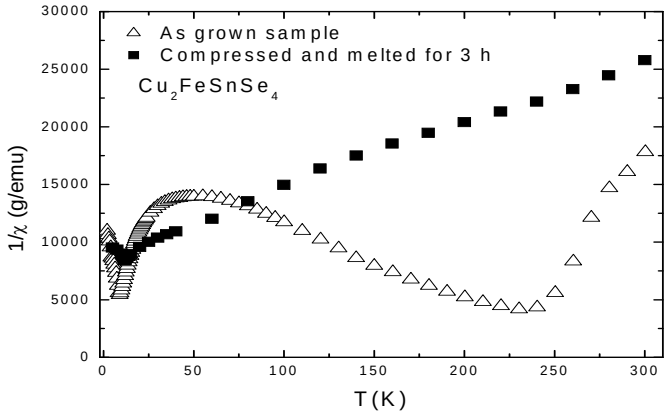

Fig. 2. Variation of the inverse of the susceptibility $1/\chi$ with temperature T for z=1, $Cu_2FeSnSe_4$. Triangles: as grown sample. Squares: compressed and melted for 3 h.

While that this minimum is considerably reduced for the compressed sample melted for 3 h, so that the effect from $FeSe_2$ is negligible in the present analysis. Details of the magnetic measurements obtained for the present alloys will be given in a further work.

3. Results and discussion

Samples of $Cu_2Cd_{1-z}Fe_zSnSe_4$ were prepared, in steps of approximately 0.1 in z, as indicated above. With regard to the X-ray and Rietveld refinement results, typical observed and theoretical x-ray diffraction spectra as well as the difference diagrams obtained for samples with z=0.2 and z=0.8 are, respectively, shown in figs. 3 and 4.

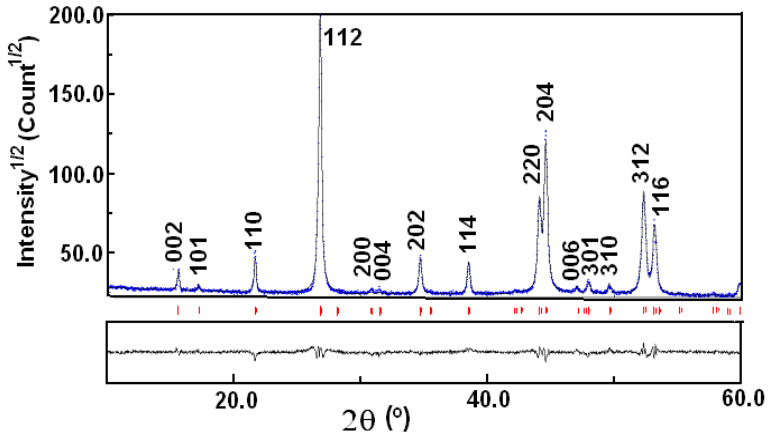

Fig. 3. Typical experimental, calculated and difference X-ray powder diffractograms for the $Cu_2Cd_{1-z}Fe_zSnSe_4$ system with z= 0.2, the hkl indices are also shown.

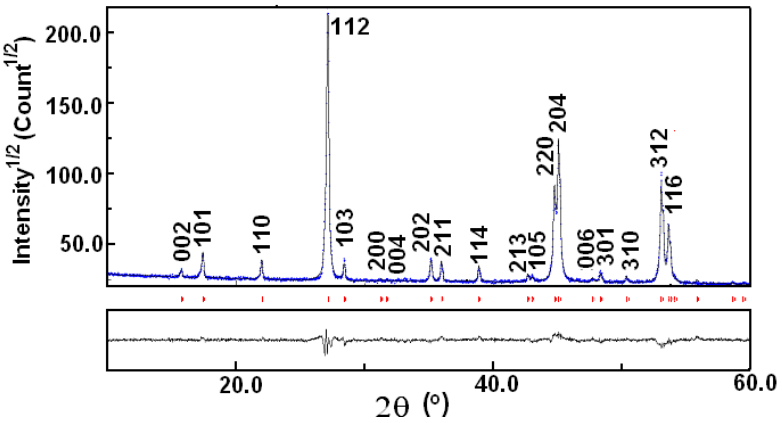

Fig. 4. Typical experimental, calculated and difference X-ray powder diffractograms for the $Cu_2Cd_{1-z}Fe_zSnSe_4$ system with z=0.8, the hkl indices are also shown.

The Rietveld structural refinement results will be given below. It was found that, at room temperature, the stannite structure occurs across the whole composition range. Also, it appeared that, because of the scattering powers of Cu and Fe are very different than the one for Cd and/or Sn atoms, Cd and Sn being similar, the intensity of the ordering lines from the tetragonal stannite structure, such as the (101), (103), (211), etc. lines, decreases as the composition z is decreased, and these lines could not be detected for samples with z<0.25. However, it is found that line splitting, viz. [(220, 204)], [(312, 116)], etc., due to tetragonal distortion $\boldsymbol{c/a} < 2$ of the stannite structure, is observed across the whole composition range, the separation of the splittings decreases as the composition z is increased, these results are illustrated in figs. 3 and 4. Values of the crystallographic parameters ***a*** and ***c*** were estimated and then refined as indicated above and the resulting values are shown in fig. 5. It is found that the values of ***c/a*** increase nonlinearly from about 1.955 for z=0 to 1.975 for z=1. The crystal parameter values obtaine for the compounds are in agreement with those given in earlier works [5, 13, 14, 15].

Turning to the Rietveld study, the results of the calculation as well as the experimental X-ray conditions are summarized in table 1, and the final atomic positions are given in table 2. The selected bond distances and angles are listed in table 3. In the present tetrahedrally coordinated stannite structure ($I\bar{4}2m$), each Se anion is surrounded by four cationic sites, i.e. two Cu, one Sn and one M, where the mixed cation M is given as M=(1-z)Cd + zFe, and each cation is similarly coordinated by four Se atoms. Moreover, the Cd, Fe and/or M ions share the z=0 and z=1/2 cation layers with Sn. The values of the anion Se displacement parameters $\Delta x_{Se}=\Delta y_{Se}$ (=1/4-x_{Se}) and Δz_{Se} (=1/8-z_{Se}) are shown plotted as a function of z in figs. 6.

Table 2. Atomic coordinates for the system $Cu_2Cd_{1-z}Fe_zSnSe_4$.

			$Cu_2Cd_{0.9}Fe_{0.1}SnSe_4$				$Cu_2Cd_{0.8}Fe_{0.2}SnSe_4$				$Cu_2Cd_{0.7}Fe_{0.3}SnSe_4$			
Atom	**Ox.**	**Site.**	***x***	***y***	***z***	**Foc**	***x***	***y***	***z***	**Foc**	***x***	***y***	***z***	**F**
Cu	+1	4d	0.0	0.5	0.250	1.0	0.0	0.5	0.250	1.0	0.0	0.5	0.250	1
Cd	+2	2a	0.0	0.0	0.0	0.9	0.0	0.0	0.0	0.8	0.0	0.0	0.0	0
Fe	+2	2a	0.0	0.0	0.0	0.1	0.0	0.0	0.0	0.2	0.0	0.0	0.0	0
Sn	+4	2b	0.0	0.0	0.5	1.0	0.0	0.0	0.5	1.0	0.0	0.0	0.5	1
Se	-2	8i	0.2608(5)	0.2608(5)	0.1326(2)	1.0	0.2604(4)	0.2604(4)	0.1329(2)	1.0	0.2576(8)	0.2576(8)	0.1334(3)	1

			$Cu_2Cd_{0.5}Fe_{0.5}SnSe_4$				$Cu_2Cd_{0.4}Fe_{0.6}SnSe_4$				$Cu_2Cd_{0.3}Fe_{0.7}SnSe_4$			
Atom	**Ox.**	**Site.**	***x***	***y***	***z***	**Foc**	***x***	***y***	***z***	**Foc**	***x***	***y***	***z***	**Foc**
Cu	+1	4d	0.0	0.5	0.250	1.0	0.0	0.5	0.250	1.0	0.0	0.5	0.250	1.0
Cd	+2	2a	0.0	0.0	0.0	0.5	0.0	0.0	0.0	0.4	0.0	0.0	0.0	0.3
Fe	+2	2a	0.0	0.0	0.0	0.5	0.0	0.0	0.0	0.6	0.0	0.0	0.0	0.7
Sn	+4	2b	0.0	0.0	0.5	1.0	0.0	0.0	0.5	1.0	0.0	0.0	0.5	1.0
Se	-2	8i	0.2475(5)	0.2475(5)	0.1319(3)	1.0	0.2458(4)	0.2458(4)	0.1314(2)	1.0	0.2432(3)	0.2432(3)	0.1312(2)	1.0

			$Cu_2Cd_{0.1}Fe_{0.9}SnSe_4$				$Cu_2FeSnSe_4$			
Atom	**Ox.**	**Site.**	***x***	***y***	***z***	**Foc**	***x***	***y***	***z***	**Foc**
Cu	+1	4d	0.0	0.5	0.250	1.0	0.0	0.5	0.250	1.0
Cd	+2	2a	0.0	0.0	0.0	0.1	0.0	0.0	0.0	0.0
Fe	+2	2a	0.0	0.0	0.0	0.9	0.0	0.0	0.0	1.0
Sn	+4	2b	0.0	0.0	0.5	1.0	0.0	0.0	0.5	1.0
Se	-2	8i	0.2415(4)	0.2415(4)	0.1298(3)	1.0	0.2419(5)	0.2419(5)	0.1298(3)	1.0

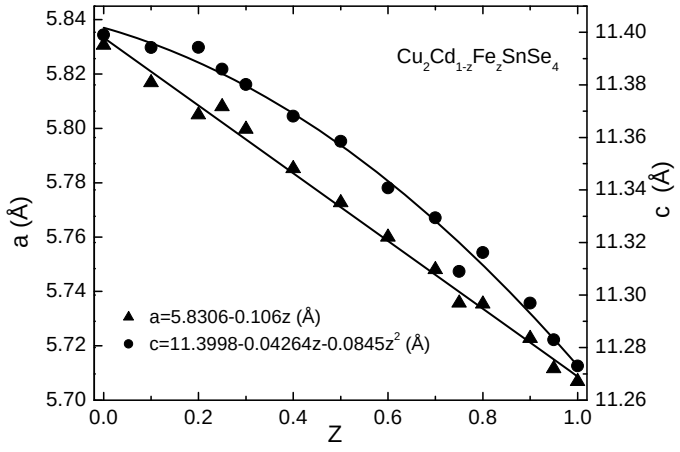

Fig. 5. Variation of lattice a and c with composition z. Full triangles: a; full circles: c. In each case, the fitted line is generated by the resulting least squared equation indicated in the inset.

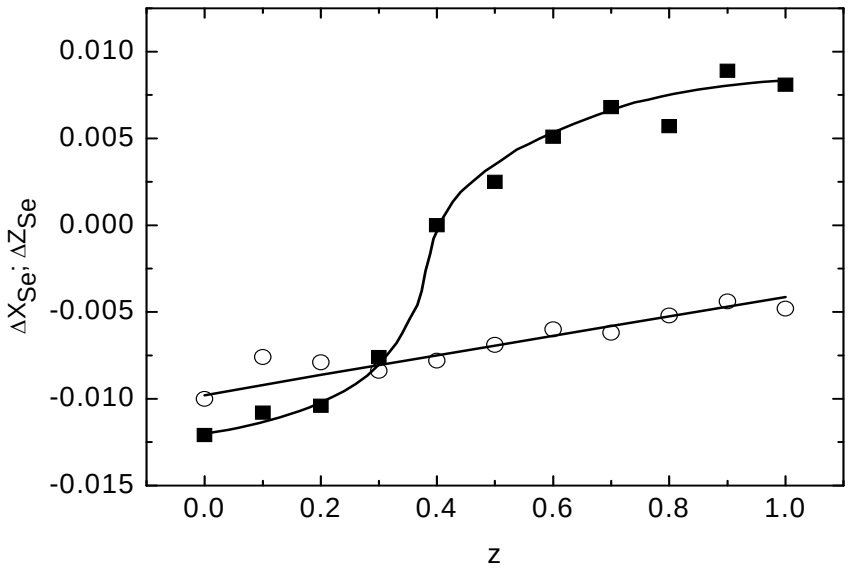

Fig. 6. Variation of anion Se displacement parameters $\Delta x_{Se}=\Delta y_{Se}$ (=1/4-x_{Se}) and Δz_{Se} (=1/8-z_{Se}) with composition z for $Cu_2Cd_{1-z}Fe_zSnSe_4$. Squares: Δx_{Se}; circles: Δz_{Se}. Values for $Cu_2CdSnSe_4$ taken from Ref. 14. The lines are to guide the eyes.

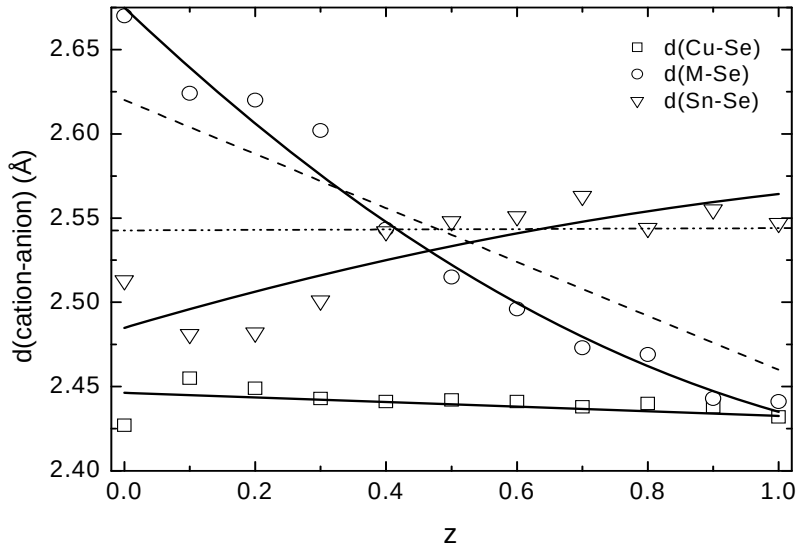

Fig. 7. Variation of cation-anion bond distances for $Cu_2Cd_{1-z}Fe_zSnSe_4$. Squares: d(Cu-Se); circles: d(M-Se); triangles: d(Sn-Se). Dashed line: d(M-Se) distance obtained from adding the tetrahedral Paling radii. Horizontal dash dotted line: d(Sn-Se) distance obtained from adding the tetrahedral Paling radii. Values for $Cu_2CdSnSe_4$ taken from Ref. 14. The solid lines are to guide the eyes.

The composition variations of the bond distances d(Cu-Se), d(M-Se) and d(Sn-Se) are given in fig. 7. It is seen from fig. 6 that, within the limits of the experimental errors, the absolute values of Δz_{Se} decrease linearly as z is increased. This behavior is consistent with the decrease of the line splitting observed in the x-ray results, figs. 3 and 4, and the corresponding increase of the

ratio ***c/a*** with z. It is seen in fig. 6 that the absolute value of Δx_{Se} decreases nonlinearly between z=0 and z=0.4, and then increases, again nonlinearly, from z=0.4 to z=1, resulting, in the overall range, in an S-shape curve.

Table 3. Selected bond distances (Å) and angles (°) for the system $Cu_2Cd_{1-z}Fe_zSnSe_4$.

	$Cu_2Cd_{0.9}Fe_{0.1}SnSe_4$	$Cu_2Cd_{0.8}Fe_{0.2}SnSe_4$	$Cu_2Cd_{0.7}Fe_{0.3}SnSe_4$	$Cu_2Cd_{0.6}Fe_{0.4}SnSe_4$	$Cu_2Cd_{0.5}Fe_{0.5}SnSe_4$
Cu-Se	2.455(5)	2.449(5)	2.443(5)	2.441(3)	2.442(3)
Se-M	2.624(5)	2.620(5)	2.602(5)	2.542(3)	2.515(3)
Sn-Se	2.481(6)	2.482(6)	2.501(6)	2.542(3)	2.548(3)
Se-Cu-Se	107.27(1) 113.96(1)	107.26(1) 113.99(1)	107.16(1) 114.21(1)	107.33(1) 113.85(1)	107.56(1) 113.37(1)
Se-M-Se	109.36(1) 109.69(1)	109.38(1) 109.52(1)	108.60(1) 109.91(1)	107.14(1) 110.65(1)	106.89(1) 110.78(1)
Se-Sn-Se	104.96(1) 111.77(1)	104.82(1) 111.85(1)	105.27(1) 111.61(1)	107.14(1) 110.65(1)	107.98(1) 110.22(1)

	$Cu_2Cd_{0.4}Fe_{0.6}SnSe_4$	$Cu_2Cd_{0.3}Fe_{0.7}SnSe_4$	$Cu_2Cd_{0.2}Fe_{0.8}SnSe_4$	$Cu_2Cd_{0.1}Fe_{0.9}SnSe_4$	$Cu_2FeSnSe_4$
Cu-Se	2.441(2)	2.438(2)	2.440(5)	2.438(3)	2.432(3)
Se-M	2.496(2)	2.473(2)	2.469(5)	2.443(3)	2.441(3)
Sn-Se	2.551(2)	2.563(2)	2.544(6)	2.555(3)	2.547(3)
Se-Cu-Se	107.68(1) 113.12(1)	107.74(1) 112.99(1)	107.99(1) 112.48(1)	108.08(1) 112.30(1)	108.10(1) 112.25(1)
Se-M-Se	106.68(1) 110.88(1)	106.12(1) 111.17(1)	106.73(1) 110.86(1)	106.24(1) 111.11(1)	106.29(1) 111.09(1)
Se-Sn-Se	108.52(1) 109.95(1)	109.09(1) 109.66(1)	109.22(1) 109.60(1)	109.95(1) 110.20(1)	109.30(1) 109.82(1)

It can be observed in fig. 7 that the values of d(Cu-Se), d(M-Se) and d(Sn-Se) found for samples in the range z<0.4 follow the same pattern reported in earlier work for the $Cu_2CdSnSe_4$ and $Cu_2HgSnSe_4$ compounds [14], i.e. d(M-Se)>d(Sn-Se)>d(Cu-Se). But, the resulting trend d(Sn-Se)>d(M-Se)>d(Cu-Se) is obtained for samples with z>0.4, in agreement with the data reported in ref. [9] for $Cu_2Cd_{0.5}Mn_{0.5}SnSe_4$ and $Cu_2MnSnSe_4$. It is found that the value of the d(Cu-Se) bond length is slightly shorter than the respective sum of the Pauling tetrahedral radii (Cu^{1+} = 1.35 Å and Se^{2-} = 1.14 Å) [18,19]. Sachanyuk *et al*. [9] suggested that this result would correspond to the increase of the ionic contribution to the formation of the bond. In the case of the d(M-Se), the sum of the Pauling radii (Cd^{2+} = 1.48 Å and Fe^{+2} = 1.32 Å) gives the dashed line shown in fig. 7. In the case of the d(Sn-Se) (Sn^{4+} = 1.40 Å), it is observed that, for z<0.4, the experimental values are slightly lower than the Pauling sum (2.54 Å), dash dotted line in fig. 7, while that the agreement becomes better in the range 0.4<z<1. It is seen from fig. 7 that, when Cd is replaced by Fe, the d(Cu-Se) distance as well as the Se-Cu-Se angle, table 3, change very little with z, while d(M-Se) decreases by about 0.22 Å and d(Sn-Se) increases by about 0.067 Å. These results mean that, as z is increased, the size of the mixed cation M is reduced, and then M moves toward its neighboring Se anion, while the Sn cation moves far away from its Se anion, similarly the Se moves toward its neighboring M cation and far away from the Sn ion, resulting in an overall increase of the Se-M-Se and a reduction of the Se-Sn-Se angles. The obtained angles are very close to the ideal tetrahedral bond angle (109.5º). However, it appears that in the range 0<z<0.4 the tetrahedra surrounding the M cations are the most regular, while that for z>0.4 the Sn atom form a nearly perfect tetrahedron with its Se nearest neighbors. It can be seen from fig.5 that, within the limits of experimental error, while the crystallographic parameter ***a*** follows the usual linear Vegard behavior, the values of ***c*** are found to vary nonlinearly with z indicating deviations from the Vegard form for this case. This behavior would be related with the composition dependence of the internal distortion parameter, $\sigma = [(1/4\text{-}x_{Se})^2 + (1/4\text{-}y_{Se})^2 + (1/8\text{-}z_{Se})^2]^{1/2}$, illustrated in fig. 8. In this figure, the points correspond to the experimental values of σ obtained for the present $Cu_2Cd_{1-z}Fe_zSnSe_4$ system, and the dashed line represents the values for the $Cu_2Cd_{1-z}Mn_zSnSe_4$ taken from refs. [9, 14]. Thus, it is seen from this figure that the form of the σ vs z curve for the $Cu_2Cd_{1-z}Fe_zSnSe_4$ system is nonlinear showing a minimum at about z=0.4, while that for the $Cu_2Cd_{1-z}Mn_zSnSe_4$ case σ decreases linearly with z. Thus, it would be possible that, for the present chalcogenide alloy system, the nonlinear behavior of the internal parameter σ(z) would be the main reasons for the nonlinear variation of the lattice parameter ***c*** with z. It is seen that the absolute values of the obtained torsion angles (Se-M-Se-Cu) and (Se-M-Se-Sn) for cation M decrease rapidly in the range 0<z<0.4, and these values tend to level out for z>0.4, these results are illustrated in fig. 9.

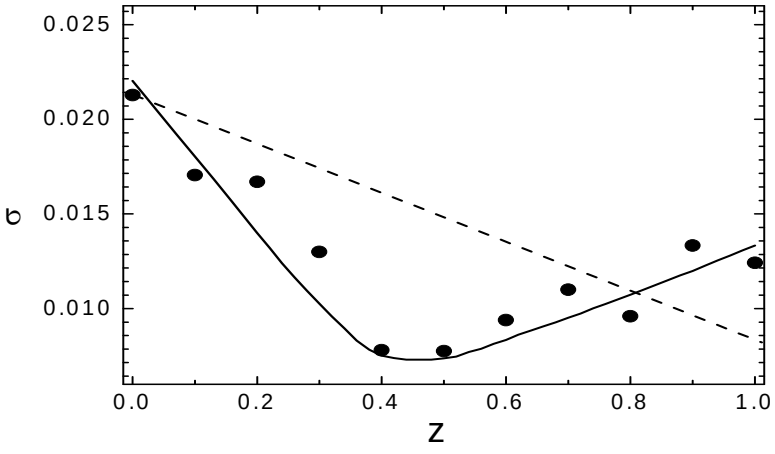

Fig. 8. $Cu_2Cd_{1-z}Fe_zSnSe_4$: variation of the internal distortion σ with composition z. The full line is to guide the eyes.

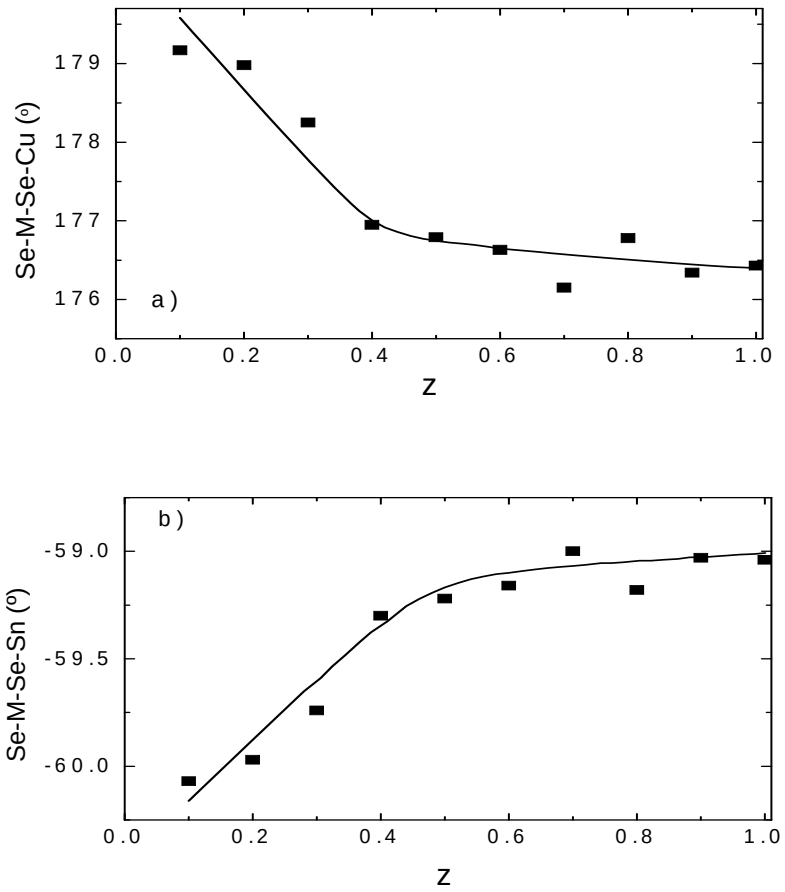

Fig. 9. Variation of torsion angles, M cation, for $Cu_2Cd_{1-z}Fe_zSnSe_4$. a) Se-M-Se-Cu, b) Se-M-Se-Sn. M=(1-z)Cd-zFe. The lines are to guide the eyes.

4. Conclusions

The resulting Rietveld refined parameters were found to be typical of the present I_2-II-IV-VI_4 materials. The deviation of the crystal parameter ***c*** from the Vegard form was related to the nonlinear variation of the internal distortion parameter σ with z. Small traces of $FeSe_2$ were observed in the range z>0.7 for the as grown samples. The magnetic measurements showed that the amounts of this extra phase were found to decrease considerably for samples which were re-melted in compressed form.

Acknowledgements

This work was partially supported by the Consejo de Desarrollo Científico, Humanistico y Tecnológico CDCHT-ULA (Projects No. C-1436-06-05-AA, C-1437-06-05-Ed, C-1547-08-05-B, C-1532-07-05-B and C-1630-09-05-B). Thanks are due to the Plan de Desarrollo de Talentos Humanos de Alto Nivel of Fondo Nacional de Ciencia, Tecnología e Investigación FONACIT, through grant No. 2008002062, Venezuela.

References

[1] Y. Shapira, E. J. McNiff Jr., N. F. Oliveira Jr., E. D. Honig., K. Dwight, A Wold., Phys. Rev. B **37**, 411 (1988).

[2] J. K Furdyna, J. Kossut, Diluted Magnetic Semiconductors, Semiconductors and Semimetals,(Edited by Willardson R. K. and Beer A. C.), Vol. 25, Chap. 1., Academic Press, New York. (1988).
[3] G. H McCabe, T. Fries, M. T. Liu, Y. Shapira, L. R. Ram-Mohan, R. Kershaw, A. Wold, C. Fau, M. Averous, E. J. Jr McNiff, Phys. Rev. B **56**, 6673 (1997).
[4] W. Shafer, R. Nitsche, Mate. Res. Bull. **9**, 645 (1974).
[5] M. Quintero, A. Barreto, P. Grima, R. Tovar, E. Quintero E., G. Sanchez Porras, J. Ruiz, J. C. Woolley, G. Lamarche, A-M. Lamarche, Mat. Res. Bull. **34**, 2263 (1999).
[6] E. Quintero, R. Tovar, M. Quintero, G.E. Delgado, M. Morocoima, D. Caldera, J. Ruiz, A. E. Mora, M. Briceño, J. L. Fernandez, J. Alloys Comp. **432**, 142 (2007).
[7] D. Caldera, M. Quintero, M. Morocoima, E. Quintero, P. Grima, N. Marchan, E. Moreno, P. Bocaranda, G. E. Delgado, A.E. Mora, M. Briceño, J. L. Fernandez, J. Alloys Comp. **457**, 221 (2008).
[8] E. Quintero, M. Quintero, E. Moreno, M. Morocoima, P. Grima, J. Henao, J. Pinilla, Journal of Alloys and Compounds, **471**(1-2), 16 (2009).
[9] V. P. Sachanyuk, I. D. Olekseyuk, O. V. Parasyuk, phys. stat. sol. (a), **203**, 459 (2006).
[10] D. Loüer, A. Boultif, J. Appl. Cryst. **24**, 987 (1991).
[11] Jean Laugier, B. Bochu, (2002). CHEKCELL: LMGP-Suite Suite of Programs for the interpretation of X-ray. Experiments, ENSP/Laboratoire des Matériaux et du Génie Physique, BP 46. 38042 Saint Martin d'Hères, France. http://www.inpg.fr/LMGP and http://www.ccp14.ac.uk/tutorial/lmgp/
[12] A. D. Mighell, C. R. Hubbard, J. K. Stalick, NBS*AIDS83: A Fortran Program for Crystallographic Data Evaluation, National Bureau of standards (USA), Tech note 1141, (1981).
[13] H. Hahn, H. Schulze, Naturwissenshaften **52**, 426 (1965).
[14] I. D. Olekseyuk, L. D. Gulay, I. V. Dydchak, L. V. Piskach, O. V. Parasyuk, O. V. Marchuk, J. Alloys Compd. **340**, 141 (2002).
[15] E. Roque-Infante, J. M. Delgado, S. A. Lopez Rivera, Mat. Letters **33**, 67 (1997).
[16] L. D. Gulay, Ya. E. Romanyuk, O. V. Parasyuk, J. Alloys Comp. **347**, 193 (2002).
[17] O. V. Parasyuk, L. D. Gulay, Ya. E. Romanyuk, L. V. Piskach, J. Alloys Comp. **329**, 202-207 (2001); Ya. E. Romanyuk, O. V. Parasyuk, J. Alloys Comp. **348**, 195-202, (2003).
[18] L. Pauling, The nature of the Chemical Bond, (Cornell University Press, Ithaca, New York, 1967), p. 246.
[19] http://www.webelements.com/copper/atom_sizes.html